Available online at www.sciencedirect.com

ScienceDirect

Current Opinion in Environmental Sustainability

Response of terrestrial evapotranspiration to Earth's greening

Zhenzhong Zeng[1,2,5], Liqing Peng[2,5] and Shilong Piao[1,3,4]

The greening of the Earth has been unequivocally observed in 30 years of satellite measurements from NOAA-AVHRR. Here, we review the recent literature on the response of terrestrial evapotranspiration (ET) to Earth's greening, including the contribution of greening to the global terrestrial ET change over recent decades and its role in the regulation by vegetation of changes in Earth's climate system. Although large uncertainties remain in the observation-based reconstructions of global terrestrial ET, all products established a significant increase in terrestrial ET over the past three decades ($P < 0.05$). The ensemble of all reconstructions over the period 1982–2011 provided a relatively robust estimate of 0.97 ± 0.16 trillion tonnes per year per decade, or 7.65 ± 1.26 mm per year per decade averaged over the terrestrial area. More than 50% of this global intensification of terrestrial ET was caused by the greening of the Earth, as evidenced by observation-based statistical analysis and observation-driven model simulations. Earth system model simulations further showed that this response is a key determinant of the complex feedback loops of Earth's greening with Earth's water and climate systems. These results highlight the need for much more accurate representation of vegetation dynamics and the sensitivity of ET to vegetation changes in Earth system models, which will ultimately improve the strategies developed for water resource management and climate change mitigation via ecosystem management.

Addresses
[1] Sino-French Institute for Earth System Science, College of Urban and Environmental Sciences, Peking University, Beijing 100871, China
[2] Department of Civil and Environmental Engineering, Princeton University, Princeton, NJ 08544, USA
[3] Key Laboratory of Alpine Ecology and Biodiversity, Institute of Tibetan Plateau Research, Chinese Academy of Sciences, Beijing 100085, China
[4] Center for Excellence in Tibetan Earth Science, Chinese Academy of Sciences, Beijing 100085, China

Corresponding author: Piao, Shilong (slpiao@pku.edu.cn)
[5] Equal contribution.

Current Opinion in Environmental Sustainability 2018, **33**:9–25

This review comes from a themed issue on **System dynamics and sustainability**

Edited by **Bojie Fu** and **Yongping Wei**

For a complete overview see the Issue and the Editorial

Available online 27th March 2018

Received: 12 December 2017; Accepted: 05 March 2018

https://doi.org/10.1016/j.cosust.2018.03.001

1877-3435/© 2018 Elsevier B.V. All rights reserved.

Introduction

The global water cycle has likely been intensified by climate change, potentially increasing the risk of hydrological hazards and threats to societies and ecosystems [1•]. Global terrestrial evapotranspiration (ET), the process of water transport from the land surface to the atmosphere, is a key component of the global water cycle [2•] and energy balance [3•], strongly shaping global rainfall, temperature, and atmospheric motion fields [4,5••]. Regional ET affects runoff, soil moisture, and groundwater, and thus the availability of water resources [6•,7•]. Local ET plays a significant role in altering the severity and duration of hydrological extremes due to agricultural and hydrological droughts, especially in transitional regions [8•]. Therefore, investigating changes in ET and the underlying mechanisms can greatly advance our understanding and modelling of land surface processes, as well as our ability to predict the alteration of the water cycle under climate change.

Terrestrial ET consists of two types of water vaporisation: (1) abiotic evaporation from open water, rainfall interception, and bare soil; and (2) biotic transpiration through diffusion of water molecules from leaves to the atmosphere via leaf stomata [9]. Changes in the rate of the former process are attributed primarily to changes in water supply (i.e. precipitation and soil moisture) and atmospheric evaporative demand (i.e. temperature, radiation, humidity, and wind speed). The latter process, transpiration, is also controlled by the physiological properties of vegetation, such as the leaf area index (LAI), leaf mass density, albedo, surface roughness, and rooting depth [10]. Because transpiration dominates total ET over land [11•,12], vegetation changes should play an important role in the global water cycle through modification of terrestrial ET.

A distinctive feature of global vegetation changes over the past 30 years is the greening of the Earth. Due to the increasing CO_2 fertilisation effects, nitrogen deposition, climate change, and land use change, the global LAI has significantly increased by 8% for 1982–2011 and the most significant increasing regions are the boreal forests in high latitudes, the tropical rainforests, the Tibetan Plateau, Sahel, India, Europe, southeast China, the eastern United States [13••]. The changes in physiology and vegetation structure associated with this greening may affect the carbon, energy, and water fluxes in terrestrial ecosystems. Significant impacts of Earth's greening on the terrestrial water cycle have been revealed using an offline diagnostic ET algorithm driven by observations [14•,15•] and

coupled Earth system model simulations [5••,16••]. Given that this greening is projected to continue in the 21st century [17,18•], understanding its impacts on ET can help us to understand how vegetation changes have affected the water cycle in recent decades, and to predict the implications for changes in the terrestrial water cycle during the 21st century.

Dickinson *et al.* [19], Moran and Jackson [20], Wang and Dickinson [21••], and Zhang *et al.* [22], among others, have reviewed previous work on the climatology and climatic variability of terrestrial ET, as well as field measurements, remote-sensing retrieval, and numerical model simulations of ET. In addition, Kool *et al.* [23•] reviewed existing methods for the measurement of ET partitioning into evaporation and transpiration, which is the main uncertainty in the modelling of land surface processes [5••]. Bosch and Hewlett [24] and Zhang *et al.* [25] reviewed the potential effects of vegetation changes on terrestrial ET. However, long-term variation in terrestrial ET and its causes have not been reviewed and remain unclear. Although all recent reconstructions of global terrestrial ET show consistent intensification over the past 30 years [14•,15•,26•–29•], large uncertainties regarding the magnitude, spatial pattern, and drivers of these ET trends remain. Building on previous knowledge, this review is centred on ET changes over recent decades, with particular focus on the response of ET to Earth's greening. In "Mechanisms of terrestrial ET and variation therein" section, we review the theoretical basis for ET processes and their drivers. In "Spatio-temporal changes in terrestrial ET over recent decades" section, we evaluate observation-based estimates of ET changes over the past few decades; "Factors intensifying terrestrial ET over recent decades" section includes attribution of ET changes to environmental factors, with a particular focus on the greening of the Earth. In "Feedbacks of the response of ET to Earth's greening with Earth's climate system" section, we discuss climate feedback due to the response of terrestrial ET to greening. The uncertainties and limitations of previous studies regarding the response of terrestrial ET to Earth's greening are then discussed in "Uncertainties and limitations" section. This review concludes in "Conclusions" section by proposing further works to advance our understanding of the response to greening and our ability to predict future terrestrial ET change.

Mechanisms of terrestrial ET and variation therein

Terrestrial ET is the exchange of water vapour between the land surface and the atmospheric boundary layer through diffusion. In the surface layer, molecular diffusion is negligible and turbulent diffusion is the primary process by which water vapour is transferred [30]. As a physical process, ET is a phase change of water from the liquid to the vapour phase, which requires substantial energy. Therefore, evaporation requires energy that allows water molecules to escape from the liquid surface and turbulent air to remove these water molecules and avoid vapour condensation [31]. Bowen [32] first linked evaporation to energy exchanges as a mass transfer process, and Penman [33] later developed a combination equation for evaporation, usually expressed as:

$$\lambda E_p = \frac{\Delta(R_n - G) + \rho_a C_p D / r_a}{\Delta + \gamma}, \quad (1)$$

where ρ_a is the air density, C_p is the specific heat of air, Δ is the slope of the saturation vapour pressure curve at the temperature of interest, and λ is the psychrometric constant or the ratio of the latent heat of vaporisation to the specific heat of air at constant pressure. Δ and γ are strong functions of air temperature. R_n is the surface net radiation, G is the surface ground heat, and the term R_n–G is sometimes referred to as available energy; lastly, r_a is the aerodynamic resistance of heat flux.

The Penman equation (Eq. (1)) is a comprehensive physics-based formula for the estimation of evaporation under sufficient water supply, namely, atmospheric evaporative demand or so-called potential evaporation (PET). Terrestrial ET is determined primarily by atmospheric evaporative demand through the climatic factors noted in the equation, including radiation, temperature, humidity, and wind speed. This linkage between ET changes and climate variability or climate change explains why terrestrial ET may change with global brightening or dimming, global warming, and stilling of winds.

Aside from atmospheric evaporative demand, terrestrial ET is also limited by biophysical conditions of the land surface. It is a function of water supply and, specifically, the soil moisture content [8•]. Under wet conditions, when soil moisture is above a critical value, ET is independent of soil moisture and is limited by incoming energy. Under water-limited conditions, when soil moisture content decreases, the soil water potential becomes more negative, and ET is reduced as the remaining soil moisture becomes less accessible via diffusion or uptake by roots. Under very dry conditions, when the soil moisture content is below the wilting point, ET is reduced to almost zero and is no longer affected by soil moisture. This separation based on soil moisture conditions provides a useful framework for the determination of ET under different climatic regimes [34], and has been employed widely in previous land surface models as a 'bucket model' [35,36], which has the general form of:

$$ET = \beta E_p \quad (2a)$$

$$\beta = \frac{\theta - \theta_{wilt}}{\theta_{crit} - \theta_{wilt}} \text{ for } \theta_{wilt} \le \theta \le \theta_{crit}, \quad (2b)$$

where θ is the soil moisture content, θ_{wilt} is the soil moisture content at which plants start to wilt, θ_{crit} is the critical soil moisture content, and E_p is the wet-surface potential ET. Soil moisture is thus an important factor controlling ET variability in transitional regimes, such as shrublands and grasslands, where water supply often becomes limiting. Due to a lack of direct observations of soil moisture at all depths and over a large area, precipitation is often used as a proxy for soil moisture.

The surface biophysical limitation of terrestrial ET is not only a function of soil moisture, but also depends on terrestrial vegetation, which links soil moisture to the atmosphere through its roots and leaf stomata. The original Penman equation was modified to account for physical controls via soil water potential and physiological controls via stomatal cells. The most familiar modification is the Penman–Monteith (P-M) equation introduced by Monteith [37], which is used to estimate the ET rate from uniform and dense vegetation cover. Under its 'big-leaf' assumption, the resistance to water vapour transfer (r_v) of the land surface can be separated into surface resistance from roots to the canopy surface in plants (r_s) and aerodynamic resistance from the canopy surface through the boundary layer (r_a). The psychrometric parameter γ in Eq. (1) is then corrected using the ratio of these resistances, $\gamma^* = [(r_s + r_a)/r_a]\gamma$, and the resulting P-M equation can be expressed as:

$$\lambda E = \frac{\Delta(R_n - G) + \rho_a C_p D/r_a}{\Delta + \gamma(1 + r_s/r_a)} \quad (3)$$

Although the P-M equation marks a shift towards use of surface resistance (r_s) and the associated stomatal resistance (r_{st}), which accommodates physiological control, estimation of this parameter remains challenging in hydrological and ecological studies. Several semi-empirical approaches based on leaf-level processes are commonly used to determine stomatal resistance (r_{st}).

The first of these approaches, the Jarvis–Stewart equation, uses a multiplicative relationship among environmental and biological controls, including photosynthetically active radiation (PAR), ambient temperature, vapour pressure deficit (VPD), leaf water potential (ψ) representing water stress, and ambient CO_2 concentration. It is stated as [38–40]:

$$\text{the Jarvis} - \text{Stewart model}: \quad g_{st} = \frac{1}{r_{st}} = g_{s\max} f(PAR) f(T_a) f(VPD) f(\Psi) f(CO_2), \quad (4)$$

where g_{st} is the inverse of stomatal resistance (r_{st}), $g_{s\max}$ is the maximum conductance when no factor limits ET, and f denotes functions with values that range from 0 to 1. $f(PAR)$ is generally an exponential function of increasing sunlight [41], so g_{st} increases with solar radiation. $f(T_a)$ increases with ambient temperature up to a species-specific critical temperature, then declines when the optimum temperature has been exceeded [40]. $f(\Psi)$ decreases with decreasing leaf water potential due to xylem cavitation [42]. $f(VPD)$ also decays with VPD, as stomata close to avoid losing water when VPD is high. Although stomata are sensitive to the atmospheric CO_2 concentration, as they open to maximise photosynthesis when the CO_2 concentration decreases, $f(CO_2)$ is considered only in long-term ET estimates because the CO_2 concentration is relatively stable over short periods. One important feature of the Jarvis–Stewart equation is that all controlling factors are assumed to be independent. Indeed, an increase in VPD reduces stomatal conductance independently of the reductions caused by extreme high temperature or low soil water potential due to dry down. However, separate measurement of stomatal sensitivity to these environmental and biological controls is difficult.

The second category of models is based on the observed linear dependence of stomatal conductance (g_{st}) on the net assimilation rate (A) for CO_2 concentration. These models can be expressed as:

$$g_{st} = mA\frac{f_D(VPD)}{c_a - c_p}, \quad (5)$$

where m is an empirical sensitivity parameter dependent on soil moisture limitation and plant type, A is the net assimilation rate (per unit of leaf area), c_a is the atmospheric CO_2 concentration, c_p is the CO_2 compensation point at which the net assimilation rate is zero, and $f_D(VPD)$ is a function of VPD. The net assimilation rate can be estimated using a photosynthesis model as the assimilation functions minus respiration [43,44]:

$$A = \min(J_E, J_C, J_S) - R_d, \quad (6)$$

where J_E is the light-limited assimilation rate when photon transport limits ribulose bisphosphate regeneration, which depends on light, absorptance, intercellular CO_2 concentration, and leaf temperature; J_C is the Rubisco enzyme-limited assimilation rate associated with Rubisco activity, intercellular CO_2 concentration, and leaf temperature; J_S is the assimilation rate limited by the export of sucrose (a product of photosynthesis), which is close to half of the maximum net assimilation rate under saturating light and CO_2 conditions; and R_d is daytime respiration in the absence of photorespiration. The most

important feature of the second category is consideration of the impact of CO_2. Models in this category include the Ball–Berry (BB) [45] model and the Leuning (LN) [46] model.

The third category of models uses an optimisation framework to link water and carbon exchanges at the leaf level. The objective function of optimisation is usually a gain function with a cost function subtracted. For example, the Katul (KT) [47] model sets the objective function to maximise leaf carbon gain and minimise water loss through the stomata. The BB, LN, and KT models can be written in the same form as Eq. (5). The main differences among them arise from their treatment of the response of g_{st} to atmospheric humidity, as follows [9]:

$$\text{the Ball}-\text{Berry (BB) model}: \quad g_{st-BB} = \frac{m_{BB}A}{c_a - c_p} \cdot RH, \tag{7a}$$

$$\text{the Leuning (LN) model}: \quad g_{st-LN} = \frac{m_{LN}A}{c_a - c_p} \cdot \left(1 + \frac{VPD}{VPD_0}\right)^{-1}, \text{ and} \tag{7b}$$

$$\text{the Katul (KT) model}: \quad g_{st-KT} = \frac{m_{KT}A}{c_a - c_p} \cdot \frac{1}{\sqrt{VPD}}, \tag{7c}$$

where RH is relative humidity and VPD_0 is a normalising constant. Another pathway towards estimation of the cost function for water loss is through plant hydraulics [48,49]. For example, the Sperry model employs the concept of hydraulic conductance and a vulnerability curve to build a hydraulic cost function to minimise water loss.

Regardless of the approach taken to the modelling of stomatal conductance (g_{st}) at the leaf level, g_{st} must be scaled up to a 'big-leaf' canopy conductance (g_c) or surface conductance (g_s) value by integrating the layer-wise stomatal conductance weighted for leaf area density, as expressed in Eq. (8a):

$$g_s = \int_0^h LAD(z) g_{st}(z)\, dz \text{ and} \tag{8a}$$

$$LAI = \int_0^h LAD(z)\, dz, \tag{8b}$$

where LAD is the leaf area density as a function of height and LAI is the green leaf area per unit of ground surface area. Because large-scale LAD profiles are generally difficult to obtain, ET remote sensing retrieval algorithms commonly employ the relationship of LAI and LAD (Eq. (8b)) [50] directly to the scaling of g_{st}. For example, canopy conductance is a linear function of LAI in MODIS ET algorithms [51,52]. However, the linear relationship between g_{st} and LAI assumes a uniform distribution of g_{st} throughout the vertical profile, and g_s will be overestimated when LAI is high. Nevertheless, Eq. (8) provides a theoretical basis for the process by which the greening of the Earth (i.e. increasing LAI) intensifies terrestrial ET.

In summary, terrestrial ET is controlled by complex biophysical processes (Figure 1). Physical control of ET can be separated into two types: atmospheric demand (as a function of radiation, temperature, humidity, and wind speed) and moisture supply (as a function of precipitation and soil moisture). Biological control is exerted primarily by vegetation (as a function of LAI, LAD, leaf water potential, and rooting depth, and varying with light, humidity, and CO_2). Physical and vegetation control are not independent. Demand and supply can directly regulate the growth of vegetation and modify vegetation's control of ET; vegetation exerts physiological control of ET through stomatal conductance, and alters physical control by intercepting light and rainfall and generating turbulence. Therefore, the relative importance of these processes, the ways in which the physical and biological mechanisms interact, and how these factors will evolve in the future remain key problems for the management of water resources and ecosystem services in a changing environment.

Spatio-temporal changes in terrestrial ET over recent decades

Many in situ techniques exist for ET measurement from local to regional spatial scales, including scintillometry, pan measurement, sap flow, weighing lysimetry, eddy covariance, energy balance (via the Bowen ratio), surface water balance, and atmospheric water balance techniques (e.g. [28•,53•]). However, none of these approaches can be used to measure global terrestrial ET directly because they require a variety of land surface parameters that are difficult to determine at a large scale. Recently, using combinations of these ground-based observations with remote sensing technology, several techniques have been developed to reconstruct global ET over the past three decades at a reasonable resolution. We summarise observation-driven reconstructions of global land ET in Table 1.

In theory, changes in ET are driven by changes in atmospheric evaporative demand associated with solar radiation, air temperature, air humidity, wind speed, water supply (precipitation, snow, and soil moisture), and physiological properties of vegetation, such as the LAI, LAD, albedo, roughness, and rooting depth (see

Figure 1

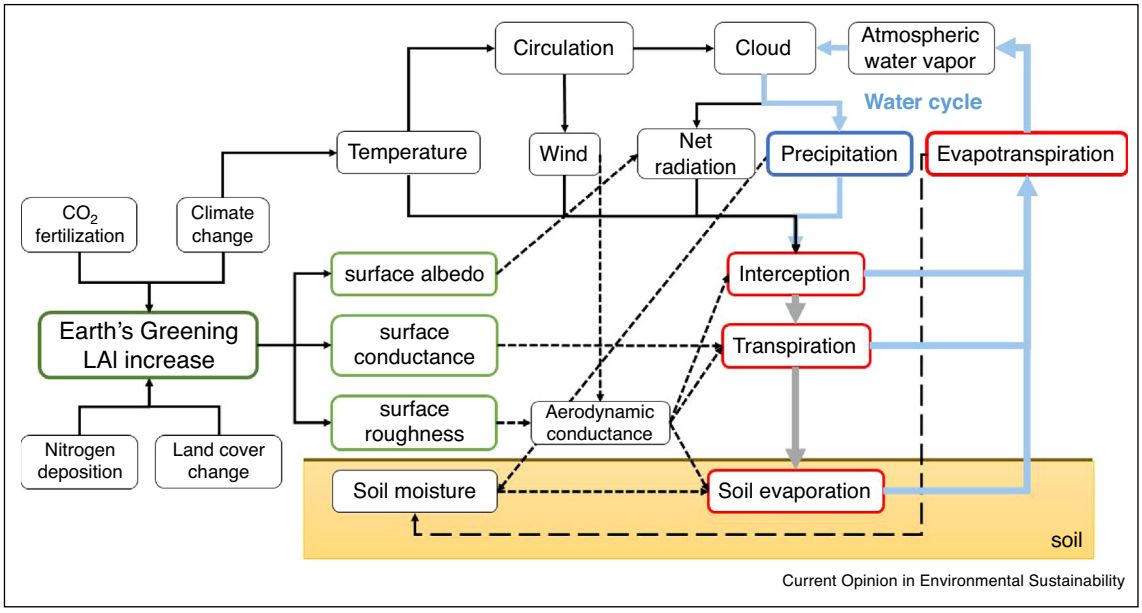

Conceptual diagram for the processes driving evapotranspiration (ET) and its interactions with other variables in the climate system, with a particular focus on the impacts of Earth greening on ET.

"Mechanisms of terrestrial ET and variation therein" section). Thus, all reconstructions of global terrestrial ET have generally included these variables as drivers of interannual variability (Table 1). Earlier reconstructions, such as WAN08 [54] and FIS08 [55], could not fully represent ET changes because they did not include water supply-related data (e.g. precipitation and/or soil moisture). The more recent JUN10 [26•] reconstruction uses precipitation as a proxy for water supply, and has shown that changes in water supply have played a key role in driving the decline of terrestrial ET trend since 1998. As JUN10 considers surface air temperature to be the only factor affecting atmospheric evaporative demand, it neglects the other important factors, such as solar radiation, humidity, and wind speed. Sheffield *et al.* [56•] noted that changing air temperature did not fully explain the change in atmospheric evaporative demand, which could be a major limitation of JUN10 and ZEN12 [28•]. ZEN14 [29•] is a data-driven global ET reconstruction similar to JUN10, but it includes basin-averaged ET values from the Gravity Recovery and Climate Experiment (GRACE) as training samples and more observations of interannual variability drivers. However, similar to JUN10, ZEN14 has uncertainties introduced by the training samples (basin-scale water balance values), the training algorithm (the model tree ensemble, a machine learning algorithm), and the observations (e.g. precipitation, temperature, radiation, and vegetation index).

Other reconstruction products have combined process-based models with observations related to atmospheric evaporative demand, water supply, and physiological properties of vegetation to physically reconstruct global land ET over recent decades (Table 1). These products include ZHA10 [27•], and later ZHA15 [14•], MU11 (i.e. MODIS ET) [52,57], VIN11 [58], YAN12 [59], ZHA16 [15•], and GLEAM [60•,61]. Among these models, ZHA10, MU11, VIN11, YAN12, ZHA15, and ZHA16 apply the revised P-M equation, whereas VIN11 and GLEAM use the revised Priestley–Taylor (P-T) equation. Vinukollu *et al.* [58] ran different models with the same forcing and found that model uncertainty (due to differences in remote-sensing estimate algorithms) could introduce large uncertainties in ET reconstructions. Besides that introduced by the remote-sensing estimate algorithms, additional uncertainty stems from the observations. For example, Vinukollu *et al.* [58] and Badgley *et al.* [62] ran the same model with different datasets and found large discrepancies among ET products.

Currently, consensus on which global ET reconstruction has the highest accuracy is lacking, due to a lack of direct observations at the global scale. All of these products have advantages and limitations, and all have been proven to be of sufficient quality for scientific research in various disciplines. Here, we review the trends in global land ET over recent decades in all representative datasets that cover the study period (1982–2011), including JUN10, ZEN14, ZHA15, ZHA16, and GLEAM (Table 1). Updated versions of the JUN10 (1982–2011) and ZEN14 (1982–2013) global ET reconstructions were used in this study. We also estimated the global trend in ET

Table 1

Summary of long-term global land ET reconstructions. Note that the drivers of interannual variability exclude variables that do not vary with year. PM, Penman–Monteith; PT, Priestley–Taylor; P, precipitation; H, surface air humidity; Ta, surface air temperature; DTaR, diurnal Ta range; Ts, land surface temperature; R, radiation; PS, pressure; Vp, vapour pressure; W, wind speed; CC, cloud coverage; Fw, wet day frequency; Ff, frost day frequency; SWE, snow water equivalent; SM, soil moisture; fAPAR, fraction of absorbed photosynthetically active radiation; NDVI, normalised difference vegetation index; EVI, enhanced vegetation index; LAI, leaf area index; SAVI, soil-adjusted vegetation index; Ve, vegetation emissivity; Va, vegetation albedo; RL, vegetation roughness length; VOD, microwave vegetation optical depth; EBBR, energy balance Bowen ratio

Product	General method	Ground-based measurements	Stomatal resistance method	Upscaling techniques	Drivers of interannual variability	Spatial resolution	Temporal resolution	Period
WAN08	Empirical method	EBBR, eddy covariance	–	Multiple regression	Ts, DTaR, R, EVI	1.0° × 1.0°	Monthly	1986–1995
FIS08	Priestley–Taylor model (PT-Fi)	Eddy covariance for validation	–	–	Ta, Vp, R, NDVI, SAVI,	1.0° × 1.0°	Monthly	1986–1993
JUN10	Data-driven	Eddy covariance	–	Model tree ensemble	P, Ta, fAPAR	0.5° × 0.5°	Monthly	1982–2008
ZHA10	Modified PM equation (PM-Zh)	Eddy covariance for parameterisation and validation; water balance for validation	The Jarvis–Stewart model	–	Ta, P, R, Vp, NDVI	8 km^2	Monthly	1983–2006
MU11	Modified PM equation for MODIS (PM-Mu)	Eddy covariance for parameterisation and validation	The Jarvis–Stewart model	–	Ta, R, H, PS, LAI, fAPAR, Va	1 km^2	8-day interval	2000–2017
VIN11	PM-Mu, PT-Fi, and the surface energy balance system (SEBS)	–	The Jarvis–Stewart model for PM-MU, – for else	–	different sources of R, P, Ts, Ta, PS, Vp, W, NDVI	0.5° × 0.5°	Daily	1984–2007
YAN12	PM method	Eddy covariance for validation	The Jarvis–Stewart model	–	R, P, Ta, DTaR, Fw, Vp, Ff, CC, LAI, RL	0.5° × 0.5°	Monthly	1982–1998
ZEN12	Empirical method	Water balance	–	Multiple regression	P, Ta, NDVI	0.5° × 0.5°	Annual	1982–2009
ZEN14	Data-driven	Water balance	–	Model tree ensemble	P, Ta, R, PS, Vp, W, Fw, Ff, NDVI	0.5° × 0.5°	Monthly	1982–2013
ZHA15	PM-Zh	–	The Jarvis–Stewart model	–	Ta, P, R, Vp, W, CO_2, NDVI	8 km^2	Daily	1982–2013
ZHA16	Penman–Monteith–Leuning method	Water balance, field experiments, eddy covariance for parameterisation and validation	The Jarvis–Stewart model	–	P, Ta, Vp, R, W, LAI, Ve, Va	0.5° × 0.5°	Daily	1981–2012
GLEAM	PT + water balance method	Eddy-covariance and soil moisture sensors for validation	–	–	R, P, Ta, SWE, VOD, SM	0.25° × 0.25°	Daily	1980–2016

using the ensemble of these products (here ensemble represents arithmetic mean; that is the annual ET averaged over the five products was used in the linear regression for the trend analysis). In addition, to provide for fair comparison of the products, we resampled all datasets at 0.5° spatial resolution and limited the study period to 1982–2011 and the study area to terrestrial areas with multiyear average LAIs > 0.1.

Global terrestrial ET was shown to have increased significantly over the past few decades, regardless of which reconstruction was selected (Figure 2). The intensification of terrestrial ET was robust, but the magnitude of the rate of increase is uncertain. The minimum rate of increase in total annual terrestrial ET over the past three decades (1982–2011) was reported by JUN10 (0.42 ± 0.12 trillion tonnes/year/decade; $P < 0.01$), and the maximum increase rate (2.16 ± 0.27 trillion tonnes/year/decade; $P < 0.01$) was documented by ZEN14. Among other global ET reconstructions, ZHA15 estimated the increase rate to be 1.35 ± 0.20 trillion tonnes per year per decade ($P < 0.01$), ZHA16 estimated it to be 0.51 ± 0.23 trillion tonnes per year per decade ($P < 0.05$), and GLEAM produced an estimate of 0.43 ± 0.17 trillion tonnes per year per decade ($P < 0.05$). An ensemble of all reconstructions provided an estimate of 0.97 ± 0.16 trillion tonnes per year per decade ($P < 0.01$), or 7.65 ± 1.26 mm yr^{-1} decade^{-1} as an average over the terrestrial area (Table 2).

In the boreal region (50–90°N), all reconstructions showed significant increases in ET ($P < 0.01$, Table 2). ZEN14 and ZHA15 suggested that significant increases in ET had occurred over all other regions ($P < 0.05$), including the tropical region (20°S–20°N), the northern temperate region (20–50°N), and the southern temperate region (20–50°S). JUN10 also recorded significant increases in ET in the tropical and northern temperate regions, but found no significant trend in the southern temperate region. Trends in the tropical, northern temperate, and southern temperate regions were positive, but not significant, in the ZHA16 and GLEAM reconstructions. The all-reconstruction ensemble estimated significant increase rates of 12.13 ± 2.39 mm yr^{-1} decade^{-1} in the tropical region, 6.04 ± 1.53 mm yr^{-1} decade^{-1} in the northern temperate region, and 5.29 ± 1.01 mm yr^{-1} decade^{-1} in the boreal region (all $P < 0.01$; Table 2). The ensemble ET trend for the southern temperate region was positive, but not significant.

At the local and regional level, the reconstructions unanimously recognised a significant increasing trend over eastern North America, Europe, boreal Asia, India, the Tibetan Plateau, southern China, eastern Latin America, southern Africa, and northern Australia ($P < 0.05$; Figure 3). The significant increase in the Tibetan Plateau has been verified by a study of this region [63]. The reconstructions also consistently showed a significant decreasing trend over the western United States. However, ET trends in other regions lack consistency (Figure 3). For example, ZEN14 and ZHA15 estimated widespread and significant increases in local ET in the Amazon (72°–48° W, 12° S–3° N; 81.7 mm yr^{-1} decade^{-1}, $P < 0.001$ for ZEN14 and 15.8 mm yr^{-1} decade^{-1}, $P < 0.001$ for

Figure 2

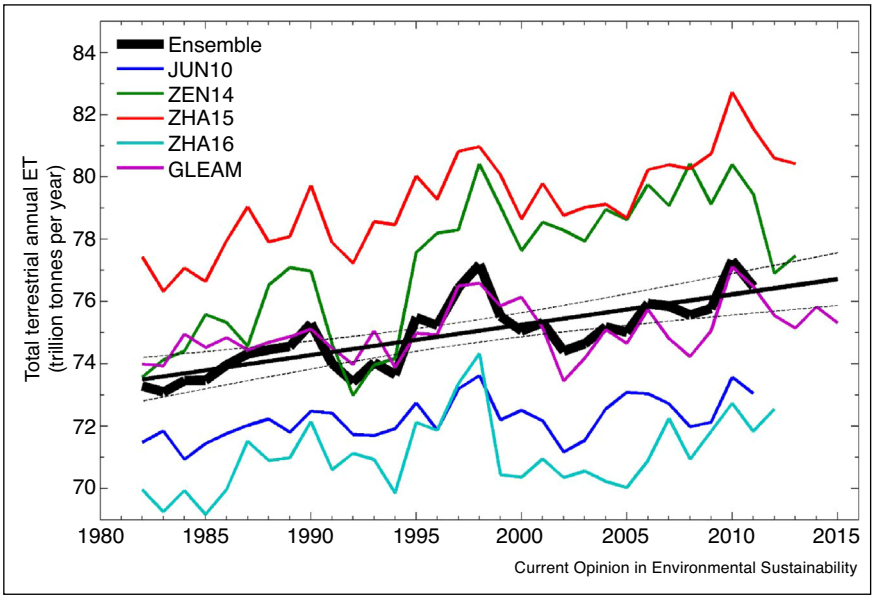

Changes in total annual terrestrial ET (trillion tonnes per year) since 1982. The coloured lines represent estimates from JUN10, ZEN14, ZHA15, ZHA16, and GLEAM. The black line is the ensemble of all estimates.

Table 2

Trends in terrestrial ET globally and in the tropical (20° S–20° N), northern temperate (20° N–50° N), southern temperate (20° S–50° S), and boreal (50° N–90° N) regions, estimated by different methods. The standard errors of these trends are also provided. The unit for all trends is mm yr^{-1} per decade

Methods	Global	Tropical (20° S–20° N)	North temperate (20° N–50° N)	South temperate (20° S–50° S)	Boreal (50° N–90° N)
Ensemble	7.65*** ± 1.26	12.13*** ± 2.39	6.04*** ± 1.53	5.16 ± 3.37	5.29*** ± 1.01
JUN10	3.30*** ± 0.96	4.35*** ± 1.47	4.05*** ± 1.23	0.17 ± 2.98	2.51*** ± 0.79
ZEN14	16.98*** ± 2.15	41.29*** ± 5.58	7.05*** ± 2.06	6.76* ± 3.64	4.02*** ± 2.14
ZHA15	10.62*** ± 1.57	13.18*** ± 2.95	12.04*** ± 1.59	9.05** ± 3.80	6.18*** ± 1.46
ZHA16	4.00** ± 1.84	0.52 ± 3.10	4.13 ± 2.47	3.06 ± 3.39	8.83*** ± 1.70
GLEAM	3.35** ± 1.37	1.34 ± 2.27	2.92 ± 1.73	6.77 ± 6.03	4.90*** ± 0.89

* indicates significance of the trends at the 90% confidence level.
** indicates significance of the trends at the 95% confidence level.
*** indicates significance of the trends at the 99% confidence level.

ZHA15, respectively), JUN10 and ZHA16 estimated non-significant trend (1.7 mm yr^{-1} decade^{-1}, $P = 0.52$ for JUN10 and 7.7 mm yr^{-1} decade^{-1}, $P = 0.26$ for ZHA16), whereas GLEAM estimated widespread and significant ET decreases (−17.7 mm yr^{-1} decade^{-1}, $P < 0.001$). In southern Latin America (77°–55° W, 25°–55° S), negative trends in local ET were documented by JUN10 (−10.8 mm yr^{-1} decade^{-1}, $P < 0.001$), ZEN14 (−10.1 mm yr^{-1} decade^{-1}, $P = 0.13$), ZHA16 (−7.6 mm yr^{-1} decade^{-1}, $P < 0.05$), and GLEAM (−12.9 mm yr^{-1} decade^{-1}, $P < 0.05$), whereas ZHA15 estimated a positive trend (12.6 mm yr^{-1} decade^{-1}, $P < 0.01$). In central Africa (17° S–40° E, 5° S–15° N), including the Sahel and Congo's rainforest, JUN10, ZEN14, and ZHA15 showed significant positive changes in local ET (9.3, 35.4, 21.8 mm yr^{-1} decade^{-1}, respectively; all with $P < 0.001$), but ZHA16 showed negative changes (−7.8 mm yr^{-1} decade^{-1}, $P < 0.1$). The large discrepancy in ET changes among reconstructions suggests the need for studies to reduce the uncertainty in ET trends in these regions. Nevertheless, the overall trend of consistently increasing ET across the globe supports the intensification of global terrestrial ET.

Factors intensifying terrestrial ET over recent decades

Terrestrial ET is driven by changes in water supply, atmospheric evaporative demand, and physiological properties of vegetation, which are often represented by precipitation, temperature, and the LAI, respectively. Figure 4 shows that the ensemble terrestrial ET is correlated significantly with variations in annual precipitation ($R = 0.66$, $P < 0.01$; time-series dataset from the Climatic Research Unit) [64], surface air temperature ($R = 0.73$, $P < 0.01$; time-series dataset from the Climatic Research Unit) [64], and the LAI ($R = 0.86$, $P < 0.01$; dataset from the third-generation Global Inventory Modeling and Mapping Studies). The overall explanation rate by these three factors is as high as 86%. We then used sensitivity analysis to separate the trend in terrestrial ET (0.97 tonnes/year/decade, $P < 0.01$) into three components induced by the individual terms. Multiple regression showed that the sensitivities of terrestrial ET to terrestrial precipitation, temperature, and LAI were 0.10 ± 0.03 tonnes yr^{-1} per mm yr^{-1} ($P < 0.01$), 0.84 ± 0.39 tonnes yr^{-1} per °C ($P < 0.05$), and 11.40 ± 1.97 tonnes yr^{-1} per m^2 m^{-2} ($P < 0.01$), respectively. Thus, increasing precipitation, temperature, and LAI led to increases in terrestrial ET of 0.22 tonnes yr^{-1} per decade ($P < 0.01$), 0.23 tonnes yr^{-1} per decade ($P < 0.01$), and 0.50 tonnes yr^{-1} per decade ($P < 0.01$), respectively. Climate change characterised by warming and increasing precipitation has been a key driving factor of the intensification of terrestrial ET over recent decades, and it explains 46% of the terrestrial ET intensification. Earth's greening appears to be a prominent driver of this trend, as it has contributed 52% of the global intensification of terrestrial ET over the past three decades.

In spatial terms, the ensemble of all reconstructions shows widespread and significant increasing trends of ET over eastern North America (95°–60° W, 25°–50° N; 9.4 mm yr^{-1} decade^{-1}, $P < 0.001$), Europe (10° W–50° E, 35°–70° N; 12.5 mm yr^{-1} decade^{-1}, $P < 0.001$), the boreal forest of Asia (35°–165° E, 50°–70° N; 6.0 mm yr^{-1} decade^{-1}, $P < 0.001$), India (67°–90° E, 7°–35° N; 15.6 mm yr^{-1} decade^{-1}, $P < 0.001$), the Tibetan Plateau (70°–100° E, 27°–43° N; 7.1 mm yr^{-1} decade^{-1}, $P < 0.001$), southern China (100°–120° E, 18°–30° N; 12.5 mm yr^{-1} decade^{-1}, $P < 0.001$), northern Latin America including the Amazon rainforest (100°–35° W, 15° S–20° N; 14.8 mm yr^{-1} decade^{-1}, $P < 0.001$), the Sahel (17° W–40° E, 5°–15° N; 16.2 mm yr^{-1} decade^{-1}, $P < 0.001$), the Congo (15°–30° E, 5° S–5° N; 9.7 mm yr^{-1} decade^{-1}, $P < 0.01$), southern Africa (11°–34° E, 25°–35° S; 12.1 mm yr^{-1} decade^{-1}, $P < 0.05$), and Southeast Asia (90°–150° E, 10° S–25° N; 10.5 mm yr^{-1} decade^{-1}, $P < 0.01$)(Figure 5a). The LAI increased in all of these regions (Figure 5b), whereas precipitation did not increase in some regions in the eastern United States, southern China, northern India, and the Amazon and Congo

Figure 3

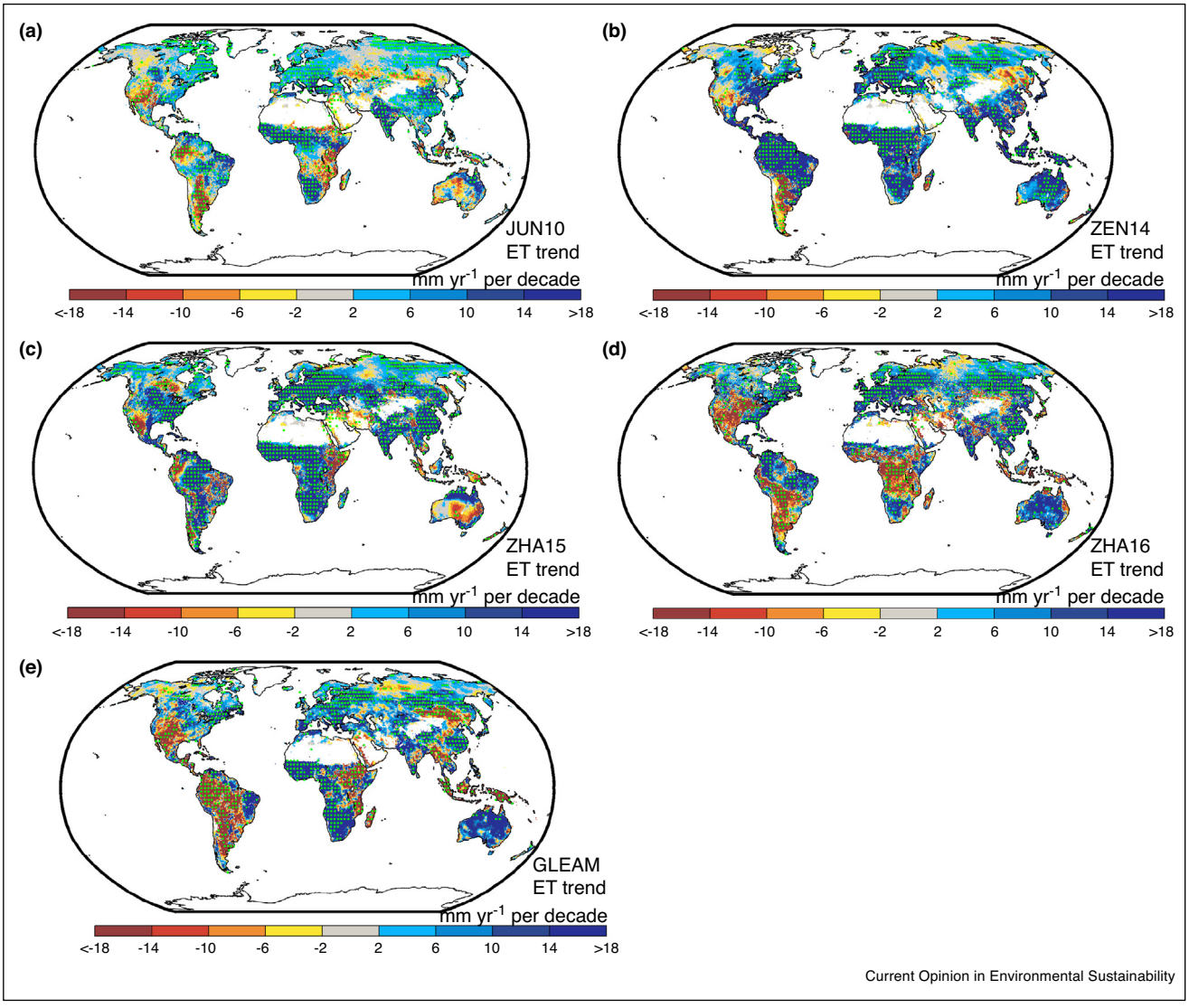

Spatial patterns of ET trends during 1982–2011 from **(a)** JUN10, **(b)** ZEN14, **(c)** ZHA15, **(d)** ZHA16, and **(e)** GLEAM. Dotting represents significant trends ($P < 0.05$).

rainforests (Figure 5c), and temperature did not increase in some regions in the eastern United States, Southeast Asia, and northern Australia (Figure 5d). The spatial consistency between ET changes and LAI changes ($R = 0.39$, $P < 0.01$; global spatial correlation controlling precipitation and temperature; Figure 5a and b) also indicates that the greening of the Earth is a prominent driver of global ET intensification. In addition, the spatial correlations between the trends of ET and LAI controlling precipitation and temperature trends are also significant ($P < 0.01$) at regional scale where positive ET trend is observed (Fig. 5a), including North America ($R = 0.47$), Europe ($R = 0.59$), the boreal forest of Asia ($R = 0.42$), India ($R = 0.46$), the Tibetan Plateau ($R = 0.33$), southern China ($R = 0.54$), northern Latin America including the Amazon rainforest ($R = 0.32$), the Sahel ($R = 0.39$), the Congo ($R = 0.38$), southern Africa ($R = 0.13$), and Southeast Asia ($R = 0.43$). Drying (decreasing precipitation) seems to be a prominent driver of the decreasing trend in ET over the western United States, southern Latin America, and eastern Africa near Madagascar (Figure 5a and c).

This correlation indicates a trend, but does not represent causality. To determine the causes of the observed terrestrial ET intensification, process-based models driven by observations could provide stronger evidence. Shi *et al.* [65] and Mao *et al.* [66] ran land surface models controlling for many environmental factors, including climate

Figure 4

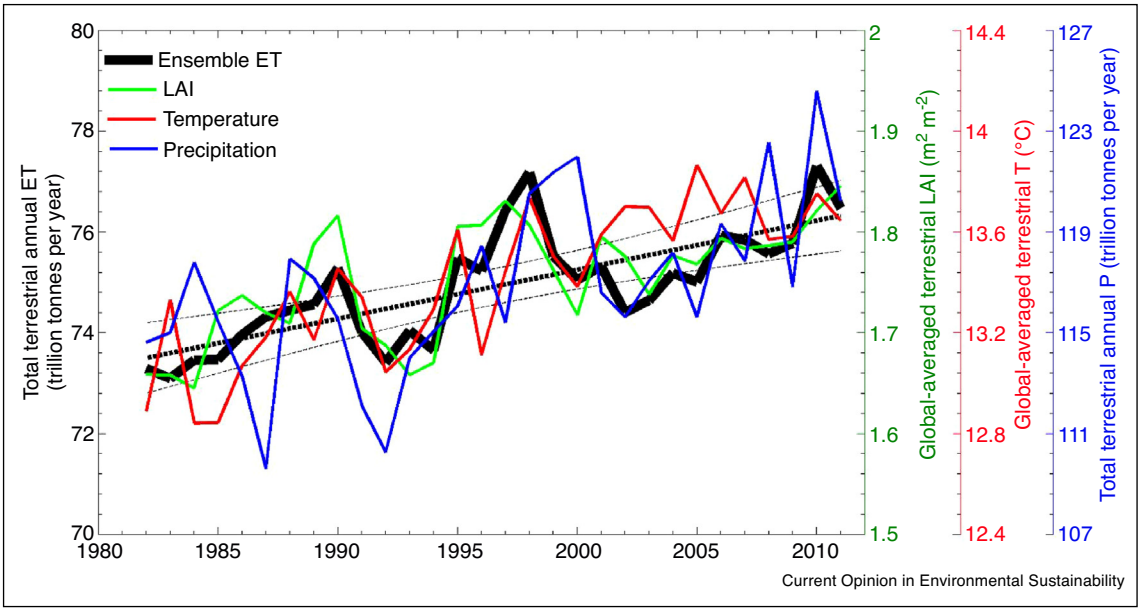

Time series of total annual terrestrial ET (trillion tonnes per year, black), global average terrestrial LAI (m^2 m^{-2}, green), global average terrestrial temperature (°C, red), and total terrestrial annual precipitation (trillion tonnes per year, blue). The straight line is the linear least squares fit line for ET.

change, increasing CO_2 concentration, nitrogen deposition, land use change, and aerosol deposition. They found that spatio-temporal variations in ET were determined mainly by climate change impacts, rather than other factors. However, neither Shi *et al.* [65] nor Mao *et al.* [66] considered the impacts of Earth's greening on the long-term ET trends. Recently, Zhang *et al.* [14•,15•] applied a remote-sensing ET model with observation-based environmental drivers, including vegetation dynamics. Their studies support the greening-induced increase in transpiration as the primary driver of increasing terrestrial ET over the last 30 years.

One limitation of using observation-driven offline algorithms for the attribution of ET changes is that these algorithms cannot disentangle the interactions among drivers, which are widespread in the observations. For example, precipitation and ET influence each other [67,68], so the increase in precipitation could be derived partly from increasing ET induced by other factors. More recently, Zeng *et al.* [5••,69] combined a land–atmosphere coupled global climate model with a long-term satellite LAI dataset to investigate the responses of the global water and climate systems (including terrestrial ET) to Earth's greening over the past 30 years. Such coupled model simulations allow consideration of the direct (increased foliar surface resulting in increased transpiration) and indirect (changes in climate due to the LAI and their feedbacks on ET) effects of LAI on ET. The authors found that Earth's greening caused an increase of 12.0 ± 2.4 mm yr^{-1} in terrestrial ET, which is about $55 \pm 25\%$ of the observed total increase in terrestrial ET over 1982–2011. Therefore, all the evidence from these observations and simulations indicates that Earth's greening has been a prominent driver of ET intensification over recent decades.

Feedbacks of the response of ET to Earth's greening with Earth's climate system

If not coupled to the atmospheric water cycle, increasing ET as a response to Earth's greening will reduce the proportion of precipitation converted into runoff, as well as water yield and soil moisture. In a coupled atmospheric and terrestrial water cycle, however, increasing ET may increase local precipitation through moisture recycling, increasing the amount of precipitation available for runoff, water yield, and soil moisture [70]. Furthermore, ET produced by surface vegetation is an important factor shaping the global temperature and motion fields in the Earth's climate system [4,71]. Because offline ET algorithms (e.g. [14•,15•,26•–29•]) have documented the intensification of terrestrial ET due to the greening of the Earth, understanding how the greening-induced increasing ET feeds back on the terrestrial water cycle and the global climate system is important. To quantify the biophysical feedbacks of Earth's greening on Earth's climate system, a coupled model rather than offline diagnostic algorithms must be used, due to the existence of strong interactions and feedbacks in Earth's climate system.

Figure 5

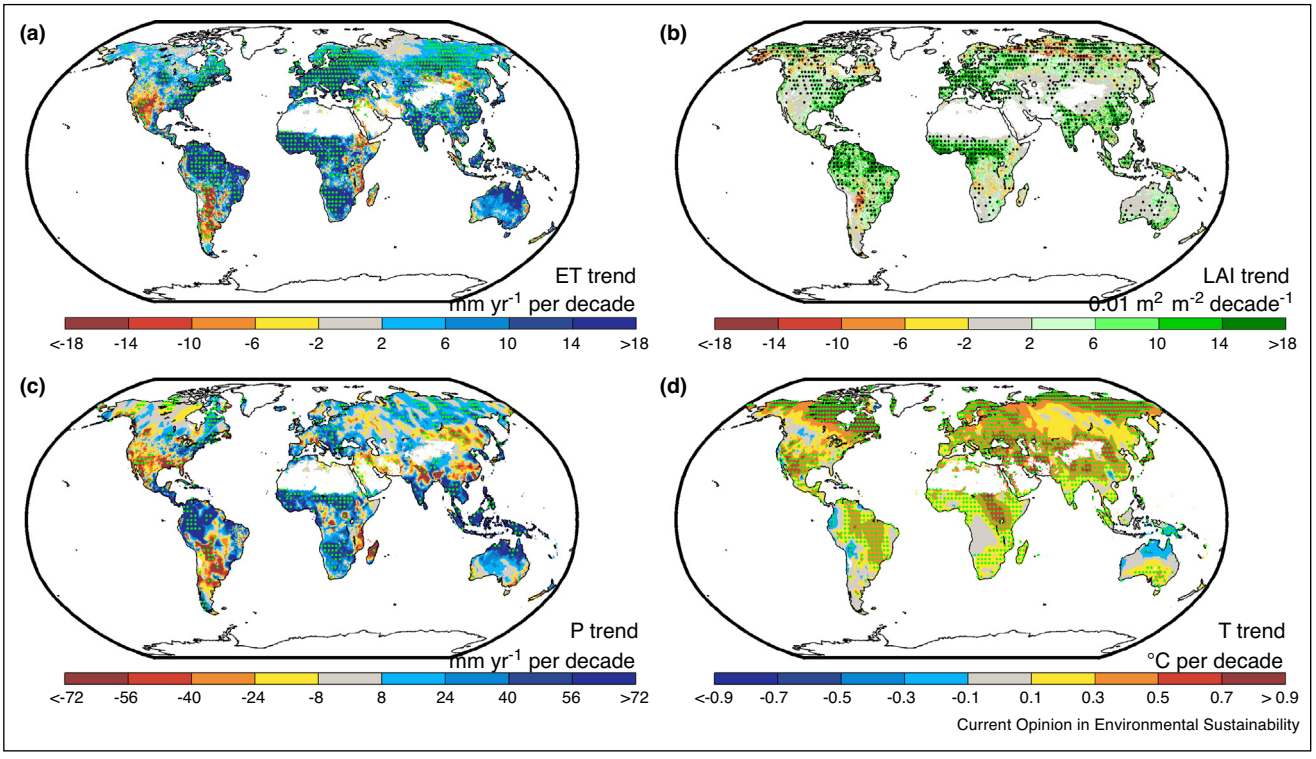

Spatial patterns of trends in **(a)** ET using the ensemble of all available products, **(b)** LAI, **(c)** precipitation, and **(d)** temperature in 1982–2011. Dotting represents significant trends ($P < 0.05$). (b) is homologous to Figure 2(b) in Zeng *et al.* [5], but in a different projection.

Zeng *et al.* [5••,69] performed coupled model simulations using state-of-the-art Earth system models combined with the satellite-observed Earth greening data. Their results indicate that the response of terrestrial ET to Earth's greening plays a fundamental role in the complex feedback loops of Earth's greening in Earth's water and climate systems. In terms of the water cycle, greening-induced terrestrial ET (12.0 ± 2.4 mm yr^{-1} from 1982 to 2011) increases the amount of atmospheric precipitable water, causing a precipitation increase of 12.1 ± 2.7 mm yr^{-1} over land, as simulated by Zeng *et al.* [69]. Increasing terrestrial ET is likely to decrease local runoff and water yield (i.e. the difference between precipitation and ET), as documented in previous studies [72•,73]. However, Zeng *et al.* [69] found that the greening of the Earth and the associated increase in ET did not significantly change runoff or water yield at a continental scale, as increasing ET also amplifies local precipitation in downwind areas. The spatial distribution of precipitation change is the key; the pattern of increasing precipitation is identical to that of increasing ET in forested (usually relatively wet) regions, such as the Amazon, the Congo basin, boreal forest regions, southern China, and Southeast Asia, possibly due to the high rates of moisture recycling. Because of the covarying changes in precipitation and ET, increasing ET did not significantly affect runoff, water yield, or soil moisture in these regions. However, in most non-forested (usually relatively dry) regions, including the Sahel, western Asia, northern India, the western United States, and the Mediterranean coast, where the pattern of precipitation is not identical to that of the greening-induced increase in ET, greening and the associated increasing ET significantly decrease soil moisture, and the progressive emergence of moisture limitation eventually halts greening-induced intensification in the water cycle. Globally, the greening of the Earth has significantly decreased soil water content by -1.41 ± 0.42 mm over the last 30 years ($P < 0.01$), dominated by greening of water-limited regions [69].

The energy required to evaporate a given amount of liquid water is approximately 600 times the energy required to increase its temperature by 1 K and 2400 times the energy required to increase the temperature of a corresponding mass of air by 1 K [8•]. A substantial amount of heat is transferred from the land surface during ET, and released into the atmosphere along with the precipitation process. Thus, increasing ET due to Earth's greening will not only alter the water cycle, but will also impact the climate system due to cooling of the land surface and influences on the atmospheric heat engine and global circulation systems [74,75]. More energy

absorbed by the land surface was dissipated due to the direct effect of increasing ET [76,77]. Over the past three decades, the greening of the Earth has led to an intensification of terrestrial ET by 3.0 ± 0.8 mm yr^{-1} per decade, and the increase in energy dissipation due to increasing ET introduces negative climate forcing at the land surface of -0.31 ± 0.07 W m^{-2} per decade [5••]. Increasing terrestrial ET also produces several indirect effects on the climate system, as it increases the input of water vapour and energy into the atmosphere. On one hand, it results in a decrease in shortwave transmissivity via changes in clouds and atmospheric water vapour, and further decreases the incoming shortwave radiation over the land surface at a rate of -0.09 ± 0.02 W m^{-2} per decade. On the other hand, as the increase in atmospheric water vapour significantly increases atmospheric air emissivity, greening-induced ET is also expected to have significantly increased downwelling longwave radiation, at a rate of 0.14 ± 0.02 W m^{-2} per decade, due to Earth's greening over the past three decades. Overall, biophysical feedbacks involving Earth's greening significantly decreased the land surface air temperature by 0.09 ± 0.02 °C over 1982–2011, primarily through the direct and indirect effects of increasing ET [5••]. Evaporative cooling from vegetation greening has been observed over the Tibetan Plateau [77] and in arid regions [78].

Uncertainties and limitations

Remote sensing observations

A large uncertainty in the estimation of the ET response to greening derives from large discrepancies among remote sensing ET products, which affect the magnitude, interannual variability, and long-term trends. For example, the interannual variability in terrestrial ET during 1982–2011 was 0.46 tonnes yr^{-1}, according to JUN10. This estimate is only 9% of the estimate from ZEN14, and only 20%, 33%, and 58% of the estimates from ZHA15, ZHA16, and GLEAM, respectively. As a result, the sensitivity of terrestrial ET to the LAI, based on multiple regression of ET and LAI data while controlling for precipitation and temperature, is only 3.9 ± 2.1 tonnes yr^{-1} per m^2 m^{-2} ($P = 0.08$) when JUN10 is chosen. This estimate is much lower than the estimates from other ET products (22% of ZEN14, 18.2 ± 2.5 tonnes yr^{-1} per m^2 m^{-2}, $P < 0.01$; 28% of ZHA15, 14.0 ± 3.5 tonnes yr^{-1} per m^2 m^{-2}, $P < 0.01$; 29% of ZHA16, 13.8 ± 4.0 tonnes yr^{-1} per m^2 m^{-2}, $P < 0.01$; and 56% of GLEAM, 7.1 ± 2.9 tonnes yr^{-1} per m^2 m^{-2}, $P < 0.05$). ZEN14 is a product similar to JUN10, as they utilise the same machine-learning algorithm to upscale, but with GRACE-based basin-averaged ET as training samples. JUN10 appears to give a lower bound of the interannual variability in terrestrial ET (and of the sensitivity of terrestrial ET to the LAI), while ZEN14 provides an upper bound. Because of the lack of ET measurements at the satellite pixel scale for validation, it is impossible to determine whether one product is superior to another one. Using an ensemble of all remote sensing ET products is a viable method to reduce the uncertainty in remote sensing ET. However, we should note that the ensemble approach is not useful for advancing our understating of physical processes or for improving ET predictions.

The collection of more direct ET measurements at ground level will not only reduce the uncertainty of remote sensing ET products, but also help to identify the combined effects of errors in remote sensing products and to optimise algorithms for global terrestrial ET. Previously, the Bowen ratio energy balance was the preferred approach for estimating regional ET at the ground level, but this approach relies strongly on the range of the Bowen ratio. In the present millennium, the eddy covariance technique has become the preferred approach to the measurement of land–atmosphere fluxes at the global scale [53•]. The major limitation of the eddy covariance technique is non-closure of the energy balance [79,80]. This technique also entails errors in the measurement of night-time ET under stable conditions [81]. In addition, eddy covariance networks are sparse in the tropics and the Southern Hemisphere, where magnitudes of ET are large [29•]. ET estimations validated elsewhere may not be accurate in these regions, particularly in tropical rainforests. Eddy covariance measurements also typically span very short periods, and the long-term global ET products based on these measurements may have space for time extrapolation biases [26•,29•].

Surface heterogeneity and scale mismatch could introduce other problems in the validation of pixel-scale satellite ET products using ground-level point-scale measurements. For example, among conventional techniques of ET measurement at ground level, lysimetry is the only one that directly measures water flux from a vegetated surface [82], but this point-level measurement is not representative of regional ET at the scale of a satellite pixel [83]. Eddy covariance measurements are useful for the validation of satellite ET products at high spatial resolution (e.g. 30 m^2, the satellite pixel of Thematic Mapper) but not at moderate to low spatial resolution (e.g. 500 m^2, the satellite pixel of MODIS). The (Extra-) Large Aperture Scintillometers use a recently developed technique to measure ET at larger scales, which could be used to validate remote sensing ET data at these scales [84,85]. In addition, the terrestrial water storage anomaly measured by the GRACE satellite and its Follow-on mission has improved and will continue to dramatically improve measurement of the terrestrial water budget at a large scale [86,87], which greatly benefits the validation of global ET products [28•,29•]. Lastly, planned satellite missions, such as NASA's Surface Water and Ocean Topography mission, will certainly improve global ET estimates in the near future [88].

The other large uncertainty in global ET estimates derives from the representative ET drivers used in the remote sensing retrieval algorithms, and their uncertainties. First, ET is driven primarily by atmospheric evaporative demand, which is associated with net radiation, air temperature, vapour pressure, and wind speed, but many studies describe evaporative demand only as a function of temperature [89,90]. Jung *et al.* [26•] and Zeng *et al.* [28•] considered temperature alone as a proxy for atmospheric evaporative demand in their algorithms. Sheffield *et al.* [56•] showed that temperature-based approaches overestimated evaporative demand and, hence, the response of ET to warming; thus, JUN10 and ZEN12 could have overestimated the temperature-driven ET change. Second, early studies did not include observations associated with interannual variations in water supply (e.g. precipitation and soil moisture); thus, the variations in those products did not represent ET changes due to the effect of water supply in reality [52,54,55,57]. Because almost all other products utilised precipitation as a proxy for soil moisture, these products cannot discern any ET changes due to soil water supply changes caused by other factors (e.g. [26•]). Lastly, changes in the physiological properties of vegetation are represented by only one or two vegetation indices in the ET remote sensing retrieval algorithms, which could be a primary source of uncertainty. The most important issue is the response of stomatal conductance to elevated CO_2, which has been neglected in almost all ET remote sensing retrieval algorithms (e.g. [26•,27•,29•,60•,61]). Stomatal conductance is likely to have decreased due to increasing water-use efficiency in response to rising CO_2 in recent decades [91•,92,93]. However, this response and the change in vegetation water-use efficiency over recent decades remain highly uncertain [94]. More field measurements are essential to confirm the physiological response of vegetation to rising atmospheric CO_2 and to consider this response in remote sensing retrieval algorithms for ET.

Numerical model simulations

Earth system models are useful for investigating how the Earth's climate has been shaped by the greening of the Earth in the past, and for predicting its future impacts. However, the model simulation results should always be treated with caution due to the limitations in representing the Earth's climate system in models, such as uncertainties in the parameterisation of land surface processes. As for the response of terrestrial ET to Earth's greening, one of the most pressing problems is the ET partitioning (T/ET) in the models, as indicated by Zeng *et al.* [5••]. In general, land surface schemes in Earth system models first simulate PET that is independent of land surface assuming sufficient surface water supply. The schemes next simulate vegetation resistance, soil resistance and interception resistance, all determined by land surface features including LAI and plant function types. The resistances are used to calculate the fractions of PET for vegetation transpiration, soil evaporation, and rainfall interception, respectively. Last, total ET is calculated as the sum of all these components. Because of the constraints of water and energy balances, total ET in different models has a similar magnitude. However, T/ET in different Earth system models varies a lot due to the uncertainties of model parameterisations and the lack of observation-based constraints [5••,11•,95,96]. The most recent isotope techniques show that T/ET should be higher than 60% [11•,12], yet most Earth system models underestimate this ratio [95] (Lian *et al.*, unpublished data). Because vegetation transpiration, soil evaporation and rainfall interception have different sensitivities to vegetation change, the errors in T/ET of the models will induce the problem of the simulated response of terrestrial ET to Earth's greening.

To quantify the biophysical climate feedbacks of Earth's greening, Zeng *et al.* [5••] ran three state-of-the-art Earth system models prescribed with the same satellite-observed LAI: the Institute Pierre Simon Laplace Coupled Earth System Model (IPSLCM); the Accelerated Climate Modeling for Energy (ACME), which is based on the Community Earth System Model; and the Australian Community Climate and Earth System Simulator coupled model (ACCESS). They found that all three models simulated an increase in transpiration with the LAI, but a significant decrease in evaporation with increasing LAI. Yet, because T/ET is seriously underestimated in ACME and ACCESS, the modelled $\partial ET/\partial LAI$ is negligible in ACME and negative in ACCESS (see Figure S10a in Zeng *et al.* [5••]). As a result, only the IPSLCM modelled a sensitivity of terrestrial ET to the LAI ($\partial ET/\partial LAI$, 0.92 ± 0.03 mm yr^{-1}/0.01 m^2 m^{-2}, $P < 0.01$) that is similar to the sensitivity estimated from satellite-derived observations (0.90 ± 0.15 mm yr^{-1}/0.01 m^2 m^{-2}, $P < 0.01$; the ensemble of observed $\partial ET/\partial LAI$ with statistical control for precipitation and temperature). Errors in the modelled $\partial ET/\partial LAI$ mean that the feedbacks of Earth's greening in Earth's climate system were also simulated improperly in the Earth system models.

Because T/ET is underestimated by many Earth system models used in the Coupled Model Intercomparison Project Phase 5 (CMIP5) [95] (Lian *et al.*, unpublished data), the modelled $\partial ET/\partial LAI$ likely is not represented reasonably in the coupled model simulations of CMIP5. Considering that the strength of feedback from vegetation in land–atmosphere interaction is determined by the response of terrestrial ET to Earth's greening in model simulations, inaccurate simulations indicate that the biophysical feedbacks of Earth's greening are not represented well in the coupled simulations of CMIP5. Zeng *et al.* [16••] evaluated the responses of terrestrial ET to Earth's greening in the CMIP5 coupled model simulations, and found biases in the modelled $\partial ET/\partial LAI$ from those models. Calibrating T/ET in the models with

observation-based T/ET [11•,12] will calibrate the modelled $\partial ET/\partial LAI$ to some extent, thereby improving the simulation of soil–vegetation–atmosphere interactions in those models.

Once $\partial ET/\partial LAI$ has been calibrated, the ability of Earth system models to simulate the greening rate ($\partial LAI/\partial t$) determines the response of terrestrial ET to Earth's greening ($\partial ET/\partial t = \partial ET/\partial LAI \cdot \partial LAI/\partial t$). However, Zeng *et al.* [69] also found that the ability of these models to simulate vegetation dynamics spans a wide range. Most Earth system models have overestimated the magnitude in recent decades compared with the satellite-observed LAI, but have underestimated the interannual variability and the trend of terrestrial average LAI. The biases in simulated LAI in the coupled models could arise for many reasons, including errors in the vegetation models, parameter uncertainties, biases in the coupling of ET with soil moisture that affects phenology, and biases in surface climate that affect growing-season length. Murray-Tortarolo *et al.* [96] and Anav *et al.* [97] evaluated the accuracy of land surface models in reproducing satellite-observed LAI for offline dynamic global vegetation models and Earth system models. They concluded that the structural errors in vegetation models were the main cause of the general overestimation of LAI magnitude in the models. The proper initialisation, distribution, and parameterisation of vegetation in the coupled models will helpimprove the representation of the dynamic behaviour of vegetation in the Earth system models [96,97].

Conclusions

The response of terrestrial ET to Earth's greening is a dominant driver of the intensification of the terrestrial water cycle during recent decades. Besides its impacts on the terrestrial water cycle, greening-induced ET influences the entire climate system by cooling the land surface and driving atmospheric precipitation recycling. Because the greening of the Earth is projected to continue in the 21st century in nearly all the state-of-the-art Earth system models involved in the CMIP5 for IPCC AR5 [17,18•], the greening-induced ET change will continue to alter the global water cycle and shape the climate system. However, large uncertainties remain in these state-of-the-art Earth system models in the simulation of dynamic vegetation changes (e.g. greening) and the sensitivity of ET to vegetation changes. To accurately simulate and predict the response of terrestrial ET to Earth's greening, we need more accurate representation of vegetation dynamics (e.g. $\partial LAI/\partial t$) and of the sensitivity of ET to LAI change ($\partial ET/\partial LAI$) in the Earth system models, which require more direct measurements at large spatial scales and over long observation periods. Ultimately, understanding and predicting the response of terrestrial ET to Earth's greening will aid the development of effective strategies for water resource management and climate change mitigation through ecosystem management.

Conflict of interest

None declared.

Acknowledgements

This study was supported by the National Natural Science Foundation of China (41561134016 and 41530528), National Youth Top-notch Talent Support Program in China, and the 111 Project (B14001).

References and recommended reading

Papers of particular interest, published within the period of review, have been highlighted as:

- • of special interest
- •• of outstanding interest

1. • Huntington TG: **Evidence for intensification of the global water cycle: review and synthesis**. *J Hydrol* 2006, **319**:83-95.
This paper reviews the historical trends in hydrologic variables and provides a set of evidence for an ongoing intensification of the water cycle.

2. • Oki T, Kanae S: **Global hydrological cycles and world water resources**. *Science* 2006, **313**:1068-1072.
The paper provides a comprehensive overview of the current state of the natural water cycle, and in particular discusses the role of climate change in determining freshwater abundance.

3. • Trenberth KE, Fasullo JT, Kiehl J: **Earth's global energy budget**. *Bull Am Meteorol Soc* 2009, **90**:311-323.
The paper provides a recent update of the Earth's global annual mean energy budget in the light of new observations and analyses.

4. Shukla J, Mintz Y: **Influence of land-surface evapotranspiration on the earth's climate**. *Science* 1982, **215**:1498-1501.

5. •• Zeng Z, Piao S, Li L, Zhou L, Ciais P, Wang T, . . . , Wang Y: **Climate mitigation from vegetation biophysical feedbacks during the past three decades**. *Nat Clim Change* 2017, **7**:432-436.
This paper integrated Earth System model simulations with Earth observations to show that conclude that the greening mitigates the Earth's climate mainly through its influence on the terrestrial hydrological cycle, particularly through land-surface evapotranspiration.

6. • Gleick PH: **Climate change, hydrology, and water resources**. *Rev Geophys* 1989, **27**:329-344.
This paper reviews state-of-the-art research into the implications of climatic changes for the hydrologic cycle and for water resources and discusses the implications of such changes for future water planning and management.

7. • Milly PC, Dunne KA, Vecchia AV: **Global pattern of trends in streamflow and water availability in a changing climate**. *Nature* 2005, **438**:347-350.
This paper provides a future projection of streamflow and water availability trends that could threaten the availability of freshwater in many regions of the world by the year 2050.

8. • Seneviratne SI, Corti T, Davin EL, Hirschi M, Jaeger EB, Lehner I, . . . , Teuling AJ: **Investigating soil moisture–climate interactions in a changing climate: a review**. *Earth Sci Rev* 2010, **99**:125-161.
This paper provides a synthesis of past research on the role of soil moisture for the climate system, in particular the role of soil moisture–temperature and soil moisture–precipitation feedbacks, and their possible modifications with climate change.

9. Katul GG, Oren R, Manzoni S, Higgins C, Parlange MB: **Evapotranspiration: a process driving mass transport and energy exchange in the soil–plant–atmosphere–climate system**. *Rev Geophys* 2012, **50**.

10. Arora V: **Modeling vegetation as a dynamic component in soil–vegetation–atmosphere transfer schemes and hydrological models**. *Rev Geophys* 2002, **40**:1-26.

11. • Jasechko S, Sharp ZD, Gibson JJ, Birks SJ, Yi Y, Fawcett PJ: **Terrestrial water fluxes dominated by transpiration**. *Nature* 2013, **496**:347-350.

This controversial paper shows that 90 percent of total terrestrial evapotranspiration are cycled through vegetation via transpiration based on the isotopic signatures of transpiration and evaporation from a global data set of large lakes.

12. Good SP, Noone D, Bowen G: **Hydrologic connectivity constrains partitioning of global terrestrial water fluxes**. *Science* 2015, **349**:175-177.

13. •• Zhu Z, Piao S, Myneni RB, Huang M, Zeng Z, Canadell JG, . . . , Cao C: **Greening of the Earth and its drivers**. *Nat Clim Change* 2016, **6**:791-795.

This paper investigates the drivers of the increasing vegetation growth trends for the past three decades using satellite data and global ecosystem models and finds that CO_2 fertilisation, nitrogen deposition, climate change, and land cover change explain 70%, 9%, 8%, and 4% of the observed greening trend, respectively.

14. • Zhang K, Kimball JS, Nemani RR, Running SW, Hong Y, Gourley JJ, Yu Z: **Vegetation greening and climate change promote multidecadal rises of global land evapotranspiration**. *Sci Rep* 2015, **5**:15956.

The paper provided an observation driven global evapotranspiration dataset over the past three decades.

15. • Zhang Y, Peña-Arancibia JL, McVicar TR, Chiew FHS, Vaze J, Liu C, . . . , Pan M: **Multi-decadal trends in global terrestrial evapotranspiration and its components**. *Sci Rep* 2016, **6**:19124.

The paper provided an observation driven global evapotranspiration dataset over the past three decades.

16. •• Zeng Z, Zhu Z, Lian X, Li L, Chen A, He X, Piao S: **Responses of land evapotranspiration to Earth's greening in CMIP5 Earth System Models**. *Environ Res Lett* 2016, **11**:104006.

The paper assessed the responses of evapotranspiration to Earth's greening in CMIP5 Earth System Models. They verified a significant and positive response of evapotranspiration to the modeled greening in each model. However, the responses were not comparable across the Earth System Models because of an inherent bias in the sensitivity of evapotranspiration to the LAI change in the models.

17. Mahowald N, Lo F, Zheng Y, Harrison L, Funk C, Lombardozzi D: **Leaf area index in Earth system models: evaluation and projections**. *Earth Syst Dyn Discuss* 2015, **6**:761-818.

18. • Mahowald N, Lo F, Zheng Y, Harrison L, Funk C, Lombardozzi D, Goodale C: **Projections of leaf area index in earth system models**. *Earth Syst Dynam* 2016, **7**:211-229.

The paper investigated the projections of LAI in the 21st century in CMIP5 model simulations.

19. Dickinson RE, Henderson-Sellers A, Rosenzweig C, Sellers PJ: **Evapotranspiration models with canopy resistance for use in climate models, a review**. *Agric For Meteorol* 1991, **54**:373-388.

20. Moran MS, Jackson RD: **Assessing the spatial distribution of evapotranspiration using remotely sensed inputs**. *J Environ Qual* 1991, **20**:725-737.

21. •• Wang K, Dickinson RE: **A review of global terrestrial evapotranspiration: Observation, modeling, climatology, and climatic variability**. *Rev Geophys* 2012, **50**:RG2005.

This paper provides a comprehensive review of the basic theories, observational methods, satellite algorithms, and land surface models for terrestrial evapotranspiration, and discusses its long-term variability and trends.

22. Zhang K, Kimball JS, Running SW: **A review of remote sensing based actual evapotranspiration estimation**. *Wiley Interdiscip Rev Water* 2016, **3**:834-853.

23. • Kool D, Agam N, Lazarovitch N, Heitman JL, Sauer TJ, Ben-Gal A: **A review of approaches for evapotranspiration partitioning**. *Agric For Meteorol* 2014, **184**:56-70.

This paper summarizes available methods currently used to separately determine evaporation and transpiration components.

24. Bosch JM, Hewlett JD: **A review of catchment experiments to determine the effect of vegetation changes on water yield and evapotranspiration**. *J Hydrol* 1982, **55**:3-23.

25. Zhang L, Dawes WR, Walker GR: **Response of mean annual evapotranspiration to vegetation changes at catchment scale**. *Water Resour Res* 2001, **37**:701-708.

26. • Jung M, Reichstein M, Ciais P, Seneviratne SI, Sheffield J, Goulden ML, . . . , Dolman AJ: **Recent decline in the global land evapotranspiration trend due to limited moisture supply**. *Nature* 2010, **467**:951-954.

The paper provided an observation driven global evapotranspiration dataset over the past three decades.

27. • Zhang K, Kimball JS, Nemani RR, Running SW: **A continuous satellite-derived global record of land surface evapotranspiration from 1983 to 2006**. *Water Resour Res* 2010, **46**:W09522.

The paper provided an observation driven global evapotranspiration dataset over the past three decades.

28. • Zeng Z, Piao S, Lin X, Yin G, Peng S, Ciais P, Myneni RB: **Global evapotranspiration over the past three decades: estimation based on the water balance equation combined with empirical models**. *Environ Res Lett* 2012, **7**:014026.

The paper provided an observation driven global evapotranspiration dataset over the past three decades.

29. • Zeng Z, Wang T, Zhou F, Ciais P, Mao J, Shi X, Piao S: **A worldwide analysis of spatiotemporal changes in water balance based evapotranspiration from 1982 to 2009**. *J Geophys Res D: Atmos* 2014, **119**:1186-1202.

The paper provided an observation driven global evapotranspiration dataset over the past three decades.

30. Shuttleworth WJ: **Putting the "vap" into evaporation**. *Hydrol Earth Syst Sci* 2007, **11**:210-244.

31. Brutsaert W: *Hydrology: An Introduction*. Cambridge University Press; 2005.

32. Bowen IS: **The ratio of heat losses by conduction and by evaporation from any water surface**. *Phys Rev* 1926, **27**:779-787.

33. Penman HL: **Natural evaporation from open water, bare soil and grass**. *Proc R Soc London Ser A* 1948, **193**:120-145.

34. Budyko: *Climate and Life*. Academic Press; 1974.

35. Manabe S: **Climate and the ocean circulation 1: the atmospheric circulation and the hydrology of the earth's surface**. *Mon Weather Rev* 1969, **97**:739-774.

36. Sellers PJ, Dickinson RE, Randall DA, Betts AK, Hall FG, Berry JA, . . . , Sato N: **Modeling the exchanges of energy, water, and carbon between continents and the atmosphere**. *Science* 1997, **275**:502-509.

37. Monteith JL: **Evaporation and environment**. *Symp Soc Exp Biol* 1965, **19**:205-233.

38. Jarvis PG: **The interpretation of the variations in leaf water potential and stomatal conductance found in canopies in the field**. *Philos Trans R Soc London Ser B* 1976, **273**:593-610.

39. Stewart JB: **Modelling surface conductance of pine forest**. *Agric For Meteorol* 1988, **43**:19-35.

40. Lhomme JP, Elguero E, Chehbouni A, Boulet G: **Stomatal control of transpiration: examination of Monteith's formulation of canopy resistance**. *Water Resour Res* 1998, **34**:2301-2308.

41. Jones HG: *Plants and Microclimate: A Quantitative Approach to Environmental Plant Physiology*. Cambridge University Press; 1992.

42. Sperry JS, Adler FR, Campbell GS, Comstock JP: **Limitation of plant water use by rhizosphere and xylem conductance: results from a model**. *Plant Cell Environ* 1998, **21**:347-359.

43. Farquhar GV, von Caemmerer SV, Berry JA: **A biochemical model of photosynthetic CO_2 assimilation in leaves of C3 species**. *Planta* 1980, **149**:78-90.

44. Collatz GJ, Ball JT, Grivet C, Berry JA: **Physiological and environmental regulation of stomatal conductance, photosynthesis and transpiration: a model that includes a laminar boundary layer**. *Agric For Meteorol* 1991, **54**:107-136.

45. Ball JT, Berry JA: **An analysis and concise description of stomatal responses to multiple environmental factors**. *Planta* 1991.

46. Leuning R: **A critical appraisal of a combined stomatal-photosynthesis model for C3 plants**. *Plant Cell Environ* 1995, **18**:339-355.

47. Katul G, Manzoni S, Palmroth S, Oren R: **A stomatal optimization theory to describe the effects of atmospheric CO_2 on leaf photosynthesis and transpiration**. *Ann Bot* 2009, **105**:431-442.

48. Sperry JS, Wang Y, Wolfe BT, Mackay DS, Anderegg WR, McDowell NG, Pockman WT: **Pragmatic hydraulic theory predicts stomatal responses to climatic water deficits**. *New Phytol* 2016, **212**:577-589.

49. Wolf A, Anderegg WR, Pacala SW: **Optimal stomatal behavior with competition for water and risk of hydraulic impairment**. *Proc Natl Acad Sci U S A* 2016, **113**:E7222-E7230.

50. Lalic B, Mihailovic DT: **An empirical relation describing leaf-area density inside the forest for environmental modeling**. *J Appl Meteor* 2004, **43**:641-645.

51. Cleugh HA, Leuning R, Mu Q, Running SW: **Regional evaporation estimates from flux tower and MODIS satellite data**. *Remote Sens Environ* 2007, **106**:285-304.

52. Mu Q, Heinsch FA, Zhao M, Running SW: **Development of a global evapotranspiration algorithm based on MODIS and global meteorology data**. *Remote Sens Environ* 2007, **111**:519-536.

53. • Baldocchi D, Falge E, Gu L, Olson R, Hollinger D, Running S, . . . , Fuentes J: **FLUXNET: a new tool to study the temporal and spatial variability of ecosystem-scale carbon dioxide, water vapor, and energy flux densities**. *Bull Am Meteorol Soc* 2001, **82**:2415-2434.
This paper introduces the technique of eddy covariance to measure the land–atmosphere exchanges of carbon, carbon and momentum.

54. Wang K, Liang S: **An improved method for estimating global evapotranspiration based on satellite determination of surface net radiation, vegetation index, temperature, and soil moisture**. *J Hydrometeorol* 2008, **9**:712-727.

55. Fisher JB, Tu KP, Baldocchi DD: **Global estimates of the land–atmosphere water flux based on monthly AVHRR and ISLSCP-II data, validated at 16 FLUXNET sites**. *Remote Sens Environ* 2008, **112**:901-919.

56. • Sheffield J, Wood EF, Roderick ML: **Little change in global drought over the past 60 years**. *Nature* 2012, **491**:435-438.
This paper shows that the inappropriate calculation of drought metrics may overestimate the drying trends on land surface.

57. Mu Q, Zhao M, Running SW: **Improvements to a MODIS global terrestrial evapotranspiration algorithm**. *Remote Sens Environ* 2011, **115**:1781-1800.

58. Vinukollu RK, Meynadier R, Sheffield J, Wood EF: **Multi-model, multi-sensor estimates of global evapotranspiration: climatology, uncertainties and trends**. *Hydrol Process* 2011, **25**:3993-4010.

59. Yan H, Wang SQ, Billesbach D, Oechel W, Zhang JH, Meyers T, . . . , Scott R: **Global estimation of evapotranspiration using a leaf area index-based surface energy and water balance model**. *Remote Sens Environ* 2012, **124**:581-595.

60. • Miralles DG, Holmes TRH, De Jeu RAM, Gash JH, Meesters AGCA, Dolman AJ: **Global land–surface evaporation estimated from satellite-based observations**. *Hydrol Earth Syst Sci* 2011, **15**:453-469.
The paper provided an observation driven global evapotranspiration dataset over the past three decades.

61. Martens B, Miralles DG, Lievens H, van der Schalie R, de Jeu RAM, Fernández-Prieto D, Verhoest NEC: **GLEAM v3: satellite-based land evaporation and root-zone soil moisture**. *Geosci Model Dev* 2017, **10**:1903-1925.

62. Badgley G, Fisher JB, Jiménez C, Tu KP, Vinukollu R: **On uncertainty in global terrestrial evapotranspiration estimates from choice of input forcing datasets**. *J Hydrometeorol* 2015, **16**:1449-1455.

63. Li X, Wang L, Chen D, Yang K, Wang A: **Seasonal evapotranspiration changes (1983–2006) of four large basins on the Tibetan Plateau**. *J Geophys Res D: Atmos* 2014, **119**:13079-13095.

64. Harris IP, Jones PD, Osborn TJ, Lister DH: **Updated high-resolution grids of monthly climatic observations – the CRU TS3. 10 dataset**. *Int J Climatol* 2014, **34**:623-642.

65. Shi X, Mao J, Thornton PE, Huang M: **Spatiotemporal patterns of evapotranspiration in response to multiple environmental factors simulated by the Community Land Model**. *Environ Res Lett* 2013, **8**:024012.

66. Mao J, Fu W, Shi X, Ricciuto D, Fisher JB, Dickinson R, . . . , Zhu Z: **Disentangling climatic and anthropogenic controls on global terrestrial evapotranspiration trends**. *Environ Res Lett* 2015, **10**:094008.

67. Bisselink B, Dolman AJ: **Recycling of moisture in Europe: contribution of evaporation to variability in very wet and dry years**. *Hydrol Earth Syst Sci* 2009, **13**:1685-1697.

68. Dirmeyer PA, Schlosser CA, Brubaker KL: **Precipitation, recycling, and land memory: an integrated analysis**. *J Hydrometeorol* 2009, **10**:278-288.

69. Zeng Z, Piao S, Li L, Wang T, Ciais P, Lian X, . . . , Myneni RR: **Impact of Earth greening on the terrestrial water cycle**. *J Clim* 2018 http://dx.doi.org/10.1175/JCLI-D-17-0236.1.

70. Spracklen DV, Arnold SR, Taylor CM: **Observations of increased tropical rainfall preceded by air passage over forests**. *Nature* 2012, **489**:282-285.

71. Bonan GB: **Forests and climate change: forcings, feedbacks, and the climate benefits of forests**. *Science* 2008, **320**:1444-1449.

72. • Jackson RB, Jobbágy EG, Avissar R, Roy SB, Barrett DJ, Cook CW, . . . , Murray BC: **Trading water for carbon with biological carbon sequestration**. *Science* 2005, **310**:1944-1947.
This paper points out the importance of considering co-benefits and trade-offs of afforestation as a carbon sequestration strategy.

73. Goulden ML, Bales RC: **Mountain runoff vulnerability to increased evapotranspiration with vegetation expansion**. *Proc Natl Acad Sci U S A* 2014, **111**:14071-14075.

74. Swann ALS, Fung IY, Chiang JCH: **Mid-latitude afforestation shifts general circulation and tropical precipitation**. *Proc Natl Acad Sci U S A* 2012, **109**:712-716.

75. Devaraju N, Bala G, Modak A: **Effects of large-scale deforestation on precipitation in the monsoon regions: remote versus local effects**. *Proc Natl Acad Sci U S A* 2015, **112**:3257-3262.

76. Peng SS, Piao S, Zeng Z, Ciais P, Zhou L, Li L, . . . , Zeng H: **Afforestation in China cools local land surface temperature**. *Proc Natl Acad Sci U S A* 2014, **111**:2915-2919.

77. Shen M, Piao S, Jeong SJ, Zhou L, Zeng Z, Ciais P, . . . , Yao T: **Evaporative cooling over the Tibetan Plateau induced by vegetation growth**. *Proc Natl Acad Sci U S A* 2015, **112**:9299-9304.

78. Forzieri G, Alkama R, Miralles DG, Cescatti A: **Satellites reveal contrasting responses of regional climate to the widespread greening of Earth**. *Science* 2017, **356**:1180-1184.

79. Wilson K, Goldstein A, Falge E, Aubinet M, Baldocchi D, Berbigier P, . . . , Verma S: **Energy balance closure at FLUXNET sites**. *Agric For Meteorol* 2002, **113**:223-243.

80. Foken T: **The energy balance closure problem: an overview**. *Ecol Appl* 2008, **18**:1351-1367.

81. Gurney RJ, Camillo PJ: **Modelling daily evapotranspiration using remotely sensed data**. *J Hydrol* 1984, **69**:305-324.

82. Li ZL, Tang R, Wan Z, Bi Y, Zhou C, Tang B, . . . , Zhang X: **A review of current methodologies for regional evapotranspiration estimation from remotely sensed data**. *Sensors* 2009, **9**:3801-3853.

83. Kairu ENDR: **A review of methods for estimating evapotranspiration particularly those that utilize remote sensing**. *GeoJournal* 1991, **25**:371-376.

84. Hoedjes JC, Chehbouni A, Ezzahar J, Escadafal R, De Bruin HA: **Comparison of large aperture scintillometer and eddy covariance measurements: can thermal infrared data be used to capture footprint-induced differences?** *J Hydrometeorol* 2007, **8**:144-159.

85. Valayamkunnath P, Sridhar V, Zhao W, Allen RG: **Intercomparison of surface energy fluxes, soil moisture, and evapotranspiration from eddy covariance, large-aperture scintillometer, and modeling across three ecosystems in a semiarid climate**. *Agric For Meteorol* 2018, **248**:22-47.

86. Wahr J, Molenaar M, Bryan F: **Time variability of the Earth's gravity field: hydrological and oceanic effects and their possible detection using GRACE**. *J Geophys Res* 1998, **103**:30205-30229.

87. Wahr J, Swenson S, Zlotnicki V, Velicogna I: **Time-variable gravity from GRACE: first results**. *Geophys Res Lett* 2004, **31**: L11501.

88. Durand M, Fu LL, Lettenmaier DP, Alsdorf DE, Rodriguez E, Esteban-Fernandez D: **The surface water and ocean topography mission: observing terrestrial surface water and oceanic submesoscale eddies**. *Proc IEEE* 2010, **98**:766-779.

89. Thornthwaite CW: **An approach toward a rational classification of climate**. *Geog Rev* 1948, **38**:55-94.

90. Monteith JL: **Evaporation and surface temperature**. *Q J R Meteorolog Soc* 1981, **107**:1-27.

91. Field CB, Jackson RB, Mooney HA: **Stomatal responses to increased CO_2: implications from the plant to the global scale**. *Plant Cell Environ* 1995, **18**:1214-1225.

• This paper introduces the consequences of increased atmospheric CO_2 from the plant to the global scale and discusses the implications for regions.

92. Drake BG, Gonzàlez-Meler MA, Long SP: **More efficient plants: a consequence of rising atmospheric CO_2?** *Annu Rev Plant Biol* 1997, **48**:609-639.

93. Medlyn BE, Barton CVM, Broadmeadow MSJ, Ceulemans R, De Angelis P, Forstreuter M, . . . , Jarvis PG: **Stomatal conductance of forest species after long-term exposure to elevated CO_2 concentration: a synthesis**. *New Phytol* 2001, **149**:247-264.

94. Saxe H, Cannell MGR, Johnsen Ø, Ryan MG, Vourlitis G: **Tree and forest functioning in response to global warming**. *New Phytol* 2001, **149**:369-399.

95. Schlesinger WH, Jasechko S: **Transpiration in the global water cycle**. *Agric For Meteorol* 2014, **189-190**:115-117.

96. Murray-Tortarolo G, Anav A, Friedlingstein P, Sitch S, Piao S, Zhu Z, . . . , Zeng N: **Evaluation of land surface models in reproducing satellite-derived LAI over the high-latitude northern hemisphere. Part I: uncoupled DGVMs**. *Remote Sens* 2013, **5**:4819.

97. Anav A, Murray-Tortarolo G, Friedlingstein P, Sitch S, Piao S, Zhu Z: **Evaluation of land surface models in reproducing satellite Derived leaf area index over the high-latitude northern hemisphere. Part II: Earth system models**. *Remote Sens* 2013, **5**:3637-3661.